JCTC Journal of Chemical Theory and Computation

pubs.acs.org/JCTC Article

MAP: An MP2 Accuracy Predictor for Weak Interactions from Adiabatic Connection Theory

Stefan Vuckovic,* Eduardo Fabiano, Paola Gori-Giorgi, and Kieron Burke

Cite This: J. Chem. Theory Comput. 2020, 16, 4141−4149 Read Online

ACCESS | Metrics & More | Article Recommendations | Supporting Information

ABSTRACT: Second-order Møller−Plesset perturbation theory (MP2) approximates the exact Hartree−Fock (HF) adiabatic connection (AC) curve by a straight line. Thus, by using the deviation of the exact curve from the linear behavior, we construct an indicator for the accuracy of MP2. We then use an interpolation along the HF AC to transform the exact form of our indicator into a highly practical MP2 accuracy predictor (MAP) that comes at a negligible additional computational cost. We show that this indicator is already applicable to systems that dissociate into fragments with a nondegenerate ground state, and we illustrate its usefulness by applying it to the S22 and S66 datasets.

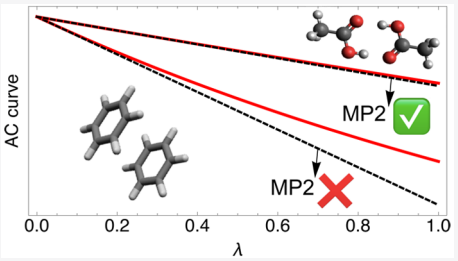

1. INTRODUCTION

The adiabatic connection (AC) formalism connects a single-particle picture to the fully interacting system in different electronic structure theories.[1−12] As such, it has played an important role in the development of both density functional theory (DFT) and wavefunction theory (WFT) methods. On the DFT side, the AC provides justification and rationalization of widely popular hybrid[13−15] and double hybrid functionals,[16−18] and it has been used for the construction of other classes of density functional approximations.[19−28] A simple geometric construction of the AC curve has been used to obtain a lower bound to the correlation energy in DFT,[24] and it has been used to rationalize the amount of exact exchange in the widely used PBE0 hybrid functional.[14,29] On the WFT side, correlation enegies from the Møller−Plesset perturbation theory arise from the weak-interaction expansion of the the Hartree−Fock (HF) AC.[30] It was also recently proposed how the AC formalism can be used to recover missing correlation energy for a broad range of multireference WFTs.[12,31,32]

In the present paper, we use the AC formalism to gain more insights into the performance of second-order perturbation theory, and in the spirit of existing quantum-chemical diagnostic tools,[33−35] we aim here at providing an indicator for the accuracy of second-order perturbation theories. Our construction is very simple and uses the fact that in the second order perturbation theories (PT2; in both DFT and HF variants of the AC formalism) the AC curve is approximated by a straight line, whose slope is equal to twice the PT2 correlation energy. Thus, the two PT2s are more accurate, the more linear the exact AC curve is. Following this, a remarkably simple geometric construction of the AC curves yields an indicator for the accuracy of the PT2 methods.[24] In the first part of the paper, we compare the exact HF and DFT AC curves for the helium isoelectronic series and report the corresponding values of our indicator. Then, in the rest of the paper, we use an interpolation along the HF adiabatic connection formalism to transform the exact form of our indicator into a practical tool for predicting the accuracy of MP2. We show that this tool is readily applicable to systems that dissociate into fragments with nondegenarate ground states. Applying it to the S22 and S66 datasets, we illustrate the usefulness of our indicator for predicting failures of MP2 when applied to noncovalently bonded systems.

2. THEORY

We briefly review the basics of the AC formalism in DFT and HF theory. In either theory, we define a coupling-constant λ-dependent Hamiltonian. In DFT, it reads as[4−6]

$$\hat{H}_\lambda^{\mathrm{DFT}} = \hat{T} + \lambda \hat{V}_{\mathrm{ee}} + \hat{V}_\lambda^{\mathrm{DFT}} \tag{1}$$

where $\hat{T}$ is the kinetic energy operator, and $\hat{V}_{\mathrm{ee}}$ is the electron−electron repulsion operator. The $\hat{V}_\lambda^{\mathrm{DFT}}$ operator represents a one-body potential, which forces $\Psi_\lambda^{\mathrm{DFT}}$, the ground state of eq 1, to integrate to the physical density $\rho = \rho_1$ for all λ values. At $\lambda = 1$, $\hat{V}_\lambda^{\mathrm{DFT}}$ is equal to $\hat{V}_{\mathrm{ext}}$, the (nuclear) external potential. The corresponding HF AC Hamiltonian is given by (see, e.g., refs 11 and 36)

$$\hat{H}_\lambda^{\mathrm{HF}} = \hat{T} + \hat{V}_{\mathrm{ext}} + \lambda \hat{V}_{\mathrm{ee}} + (1-\lambda)(\hat{J} + \hat{K}) \tag{2}$$

Received: January 17, 2020
Published: May 7, 2020

https://dx.doi.org/10.1021/acs.jctc.0c00049
J. Chem. Theory Comput. 2020, 16, 4141−4149

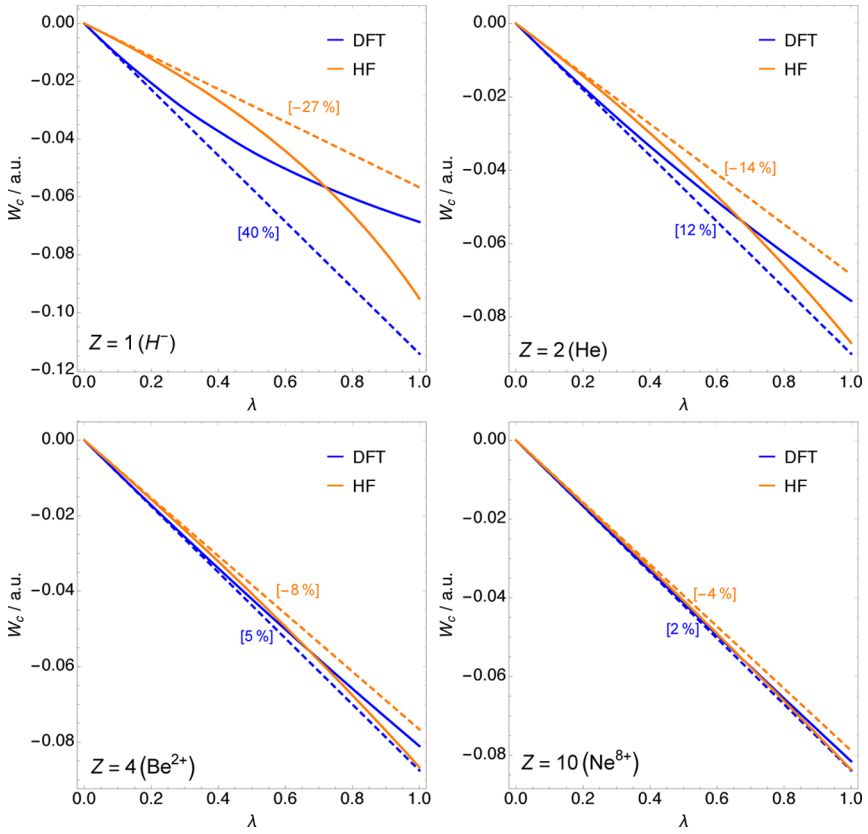

Figure 1. DFT and HF AC curves for the selected members of the helium isoelectronic series. Dashed lines represent the AC curves from the second-order perturbation theory, $2E_c^{PT2}\lambda$. The numbers in square brackets are the relative errors of E_c^{PT2}: $(E_c^{MP2} - E_c^{HF})/E_c^{HF}$ in the case of HF AC, and $(E_c^{GL2} - E_c^{DFT})/E_c^{DFT}$ in the case of DFT AC.

where $\hat{J} = \hat{J}[\rho^{HF}]$ and $\hat{K} = \hat{K}[\{\phi_i^{HF}\}]$ are the standard HF Coulomb and exchange operators, respectively, that depend on the HF density ρ^{HF} and occupied HF orbitals ϕ_i^{HF}. Thereby, these two operators are computed once in the HF calculation and do not depend on λ. The HF density arises from the HF Slater determinant, Ψ_0^{HF}, the minimizer of $\hat{H}_0^{HF}$, which is the usual Fock operator. A key difference between the two ACs is that the density of Ψ_λ^{HF} (the ground state of the Hamiltonian of eq 2) varies with λ, whereas the density of Ψ_λ^{DFT} is always forced to be that of the physical system. But at $\lambda = 1$, $\hat{H}_1^{DFT} = \hat{H}_1^{HF} = \hat{H}$, and thus, $\hat{\Psi}_1^{DFT} = \Psi_1^{HF} = \Psi$.

To avoid confusion regarding the λ-dependent Hamiltonian of eq 2, which connects the Fock operator ($\lambda = 0$) to the physical $\hat{H}$, we note that the Hartree−Fock energy of quantum chemistry simply corresponds to $\langle \Psi_0^{HF} \mid \hat{H} \mid \Psi_0^{HF} \rangle$. In either theory,

$$E_c = \langle \Psi | \hat{H} | \Psi \rangle - \langle \Psi_0 | \hat{H} | \Psi_0 \rangle \tag{3}$$

and the AC formula for the correlation energy follows in both cases from the Hellmann−Feynman theorem

$$E_c = \int_0^1 W_{c,\lambda} d\lambda \tag{4}$$

In DFT, the underlying AC integrand $W_{c,\lambda}$ is given by

$$W_{c,\lambda} = \langle \Psi_\lambda | \hat{V}_{ee} | \Psi_\lambda \rangle - \langle \Psi_0 | \hat{V}_{ee} | \Psi_0 \rangle \qquad \text{(DFT)} \tag{5}$$

whereas its HF counterpart is

$$W_{c,\lambda} = \langle \Psi_\lambda | \hat{V}_{ee} - \hat{J} - \hat{K} | \Psi_\lambda \rangle - \langle \Psi_0 | \hat{V}_{ee} - \hat{J} - \hat{K} | \Psi_0 \rangle \qquad \text{(HF)} \tag{6}$$

In DFT (eq 5), Ψ_0 is the Kohn−Sham wavefunction, and in the HF AC (eq 6), Ψ_0 is the HF Slater determinant, which minimizes $\hat{H}$. Utilizing the expansion of $W_{c,\lambda}^{DFT/HF}$ at small λ up to the n-th order, we can write

$$W_{c,\lambda}^{(n)} = \sum_{m=2}^{n} m E_c^{PTm} \lambda^{m-1} \tag{7}$$

where E_c^{PTm} is the correlation energy from the m-th order perturbation theory. The $E_c^{(n)}$ correlation energy corresponding to the AC integrand of eq 7 is then given by

$$E_c^{(n)} = \sum_{m=2}^{n} E_c^{PTm} \tag{8}$$

Within the HF AC, E_c^{PTm} is obtained from Møller−Plesset (MP) perturbation theory (PT = MP), whereas in the DFT case, E_c^{PTm} is obtained from Görling−Levy perturbation theory (PT = GL).[37,38] By truncation to the second order in λ, $W_{c,\lambda}$ is approximated by a straight line

$$W_{c,\lambda}^{DFT/HF} \approx 2E_c^{PT2}\lambda \tag{9}$$

which sets $E_c^{DFT/HF} \approx E_c^{PT2}$. Both MP2 and GL2 theories are pillars of electronic structure theory, and their use is widespread in many calculations. Besides the widespread use of the MP2 method and its extensions in their standalone versions (see, e.g., ref 39. for a review), the PT2 correlation energy is also used as an ingredient for double hybrids.[40−42]

https://dx.doi.org/10.1021/acs.jctc.0c00049
J. Chem. Theory Comput. 2020, 16, 4141−4149

3. ILLUSTRATIONS

In Figure 1, we show the AC curves in DFT and HF theory for the members of the helium isoelectronic series, namely, for H^-, He, Be^{2+}, and Ne^{8+}. For H^- and He, the second derivatives of both $W^{HF}_{c,\lambda}$ and $W^{DFT}_{c,\lambda}$ (w.r.t. λ) is plotted in Figure 1 for λ values between 0 and 2. The AC curves have been obtained from the $\Psi^{HF/DFT}_{\lambda}$ wavefunctions at the full-CI/aug-cc-pCVTZ level.[43] The DFT AC curves have been taken from refs 44 and 45, while those of the HF AC have been obtained from the Ψ^{HF}_{λ} wavefunction that we construct in the present work (the full details are given in the Supporting Information). While both AC curves decrease with λ, their convexities can be different, and that is evident from Figure 1. As it can be seen from Figure 2, $W^{DFT}_{c,\lambda}$ is convex for both systems. In fact, $W^{DFT}_{c,\lambda}$

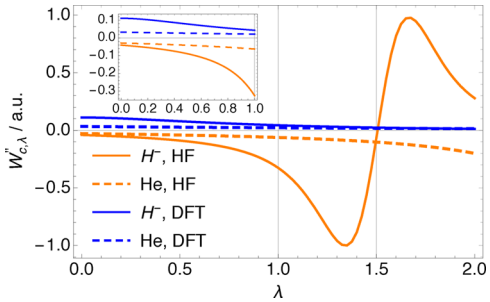

Figure 2. Curvature of the HF and DFT AC curves, $W''_{c,\lambda} = \partial^2 W_{c,\lambda}/\partial\lambda^2$, for H^- and He. The inset zooms in on the region of the plots for the λ domain between 0 and 1. The DFT AC fitting functions used in this figure are given in the Supporting Information.

is believed to be always convex (or at least piecewise convex),[24] and this is supported by the highly accurate numerical evidence.[23,44,45] On the other hand, we can see from Figure 2 that the convexity of $W^{HF}_{c,\lambda}$ is not definite. For H^-, $W^{HF}_{c,\lambda}$ is concave up to $\lambda \sim 1.5$, and then it becomes convex. For He, the convexity changes later, at $\lambda \sim 3.4$. In fact, although often concave at small λ, we know that $W^{HF}_{c,\lambda}$ must change convexity at larger λ to approach a finite asymptotic value[36] $W^{HF}_{\infty,c}$ when $\lambda \to \infty$.

Staying with Figure 1, we can notice that the curvatures of both DFT and HF AC curves are the strongest in the case of H^-, and then it decreases as we increase the nuclear charge, Z. Thus, the relative errors in the corresponding GL2/MP2 correlation energies also decrease with Z (even though the GL2 overestimates the magnitude of E^{DFT}_c here, and MP2 underestimates the magnitude of E^{HF}_c in all cases). Furthermore, the DFT and HF curves are getting closer to each other as Z increases, and for Ne^{8+}, the two curves are nearly overlapping.

4. PRACTICAL PREDICTOR FOR THE ACCURACY OF THE MP2 THEORY WHEN APPLIED TO NONCOVALENT SYSTEMS

4.1. Construction. The accuracy of E^{PT2}_c depends on how linear the exact $W_{c,\lambda}$ is. Thus, we use here a quantity defined in ref 24 as an indicator of accuracies of the two-second order perturbation theories. This indicator is defined by[24]

$$\lambda_{ext} = \frac{W_{c,1}}{W'_{c,0}} \tag{10}$$

The λ_{ext} quantity is simply a value of λ at which the extrapolated PT line ($W_{c,\lambda} = \lambda W'_0 = 2\lambda E^{PT2}_c$) reaches the $W_{c,\lambda} = W_{c,1}$ horizontal line. As such, it represents a dimensionless measure of the curvature of ACs. For the AC convex in λ (within the relevant λ region between 0 and 1), λ_{ext} needs to be less than 1. For these curves, the error of PT2 vanishes as λ_{ext} approaches 1 (from below). Thus, when the AC curve is a straight line, X is equal to 1, and the PT2 is exact. For the AC curve concave in λ (again within the relevant λ region between 0 and 1), λ_{ext} is greater than 1, and for these AC curves, the error of PT2 also vanishes when λ_{ext} approaches 1 (from above). To illustrate this, in Figure 3, we show λ_{ext} for the

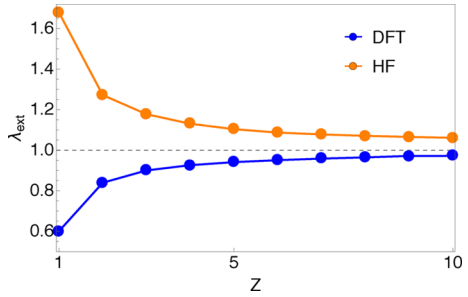

Figure 3. λ_{ext}'s for both DFT and HF AC curves for the helium isoelectronic series as a function of nuclear charge, Z.

members of the helium isoelectronic series. In the case of HF ACs, the underlying λ_{ext} value for H^- is ~1.7; for He, it drops to ~1.4, and then it further decreases with Z. In the case of DFT ACs, the underlying λ_{ext} value for H^- is ~0.6; then for He, it increases to ~0.8 and then further increases with Z. In both DFT and HF cases, λ_{ext} approaches 1 (although from different directions) as Z increases, given that both MP2 and GL2 correlation energies become exact in the large Z limit of the helium isoelectronic series.[23,38] We can also see from Figure 3 that λ_{ext} pertaining to the DFT AC approaches 1 faster than its HF counterpart. This mirrors the fact that the error of GL2 decreases more quickly than that of MP2 at larger Z (Figure 1).

So far, we have discussed the differences between the HF and DFT AC curves, and in the remainder of this paper, we focus only on HF AC, aiming to provide a practical tool for predicting the accuracy of MP2. The quantity of eq 10, via $W_{c,1}$, requires the knowledge of the fully interacting wavefunction, and thus, its direct use as an indicator for the accuracy of MP2 is impractical. We aim at circumventing this problem by obtaining $W^{HF}_{c,1}$ via interpolation between the weakly and strongly interacting limits of the ACs. This idea was proposed by Seidl and co-workers in the context of the DFT AC.[20,46] Recent papers have also explored its use in the context of the HF AC, obtaining rather good results for interaction energies, particularly[47,48] (but not only)[49] of noncovalently bonded systems. To use this approach in the HF AC context, we employ the following SPL (after Seidl, Perdew, and Levy) interpolation form[46]

$$W^{SPL}_{c,\lambda}(\mathbf{W}) = W_{c,\infty}\left(1 - \left(1 + \frac{4E^{PT2}_c\lambda}{W_{c,\infty}}\right)^{-1/2}\right) \tag{11}$$

where $\mathbf{W} = \{W^1, ..., W^k\}$ is the set of input ingredients from which the interpolation is built, which in this case is $\mathbf{W} = \{W_0, W'_0, W_\infty\}$, with $W_0 = E_x$, $W_{0'} = 2E^{PT2}_c$, and $W_{c,\infty} = W_\infty - W_0$.

https://dx.doi.org/10.1021/acs.jctc.0c00049
J. Chem. Theory Comput. 2020, 16, 4141−4149

This interpolation form has been used extensively in the literature.[23,24,28,50,51] We should immediately remark that $W^{\mathrm{SPL}}_{\mathrm{c},\lambda}$ for total energies is always convex, and as such, it cannot provide a good model for the HF adiabatic connection of a given system, and thus here, we do not attempt to build the MP2 accuracy predictor for total energies based on $W^{\mathrm{SPL}}_{\mathrm{c},\lambda}$. However, as most often in chemistry, we are interested here in interaction energies. At least for noncovalently bonded systems, interpolations like the SPL one for interaction energies work extremely well in the HF case,[47,48] pointing to the fact that the interaction energy HF adiabatic connection curve is probably, most of the times, convex and, in general, well-modeled by the difference between two convex curves, as we are going to detail in the following.

Considering a bound system (e.g., a molecular complex) M whose individual fragments are F_i, we are interested in the interaction energy AC curve, which is given by

$$W^{\mathrm{int}}_{\mathrm{c},\lambda}(M) = W_{\mathrm{c},\lambda}(M) - \sum_{i=1}^{N} W_{\mathrm{c},\lambda}(F_i) \tag{12}$$

To compute $W^{\mathrm{SPL,\,int}}_{\lambda}(M)$, we generalize the size-consistency correction of ref 48 to define

$$W^{\mathrm{SPL,int}}_{\mathrm{c},\lambda}(M) = W^{\mathrm{SPL}}_{\mathrm{c},\lambda}(\mathbf{W}(M)) - W^{\mathrm{SPL}}_{\mathrm{c},\lambda}\left(\sum_{i}^{N} \mathbf{W}(F_i)\right) \tag{13}$$

where $\mathbf{W}(M)$ and $\mathbf{W}(F_i)$ are the input ingredients of the complex and of the fragments, respectively. Eq 13 works for a system M whose fragments F_i have nondegenerate ground states; as in this case, it is guaranteed that $W^{\mathrm{SPL,\,int}}_{\mathrm{c},\lambda}(M)$ vanishes when the distance between the fragments is set to infinity. The use of eq 13 is discussed in more details in the Supporting Information.

To complete the model, we need W^{HF}_{∞}, whose exact (fully nonlocal) form has been recently revealed,[36] with ongoing efforts in exploring whether this form can be actually useful for building approximations to $E^{\mathrm{HF}}_{\mathrm{c}}$. For practical reasons here, we approximate W^{HF}_{∞} with the point-charge-plus-continuum (PC) semilocal model evaluated on $\rho^{\mathrm{HF}}(\mathbf{r})$[52]

$$W^{\mathrm{HF}}_{\infty} \approx W^{\mathrm{PC}}_{\infty}[\rho^{\mathrm{HF}}] = \int \left[A\rho^{\mathrm{HF}}(\mathbf{r})^{4/3} + B\frac{|\nabla\rho^{\mathrm{HF}}(\mathbf{r})|^2}{\rho^{\mathrm{HF}}(\mathbf{r})^{4/3}}\right]\mathrm{d}\mathbf{r} \tag{14}$$

where $A = -1.451$ and $B = 5.317 \times 10^{-3}$. The correlation part of W^{PC}_{∞} is obtained as $W^{\mathrm{PC}}_{\mathrm{c},\infty}[\rho^{\mathrm{HF}}] = W^{\mathrm{HF}}_{\infty}[\rho^{\mathrm{HF}}] - E^{\mathrm{HF}}_{\mathrm{x}}$. It has been recently shown that the combination of the PC model approximation and SPL interpolation form of eq 13 yields rather accurate interaction energies for systems that we consider in the present work.[48] In Appendix, we further discuss the use of the PC model in this context. We remark that, in addition to the SPL form, other forms have been proposed in the literature (see, e.g., refs 49 and 23). However, for the systems that we consider here, the difference between the results obtained with the SPL form and other ones is very small.[48]

Combining eqs 10, 11, and 13, we find the $\lambda^{\mathrm{SPL}}_{\mathrm{ext}}$ indicator that pertains to the interaction HF AC curve of eq 13

$$\lambda^{\mathrm{SPL}}_{\mathrm{ext}} = \frac{W^{\mathrm{SPL,int}}_{\mathrm{c},\lambda=1}(M)}{2E^{\mathrm{MP2}}_{\mathrm{c}}(M) - 2\sum_i^N E^{\mathrm{MP2}}_{\mathrm{c}}(F_i)} \tag{15}$$

where $W^{\mathrm{SPL,\,int}}_{\mathrm{c},\,\lambda\,=\,1}(M)$ is given by

$$W^{\mathrm{SPL,int}}_{\mathrm{c},\lambda=1}(M) = W^{\mathrm{PC}}_{\mathrm{c},\infty}(M)\left(1 - \left(1 + \frac{4E^{\mathrm{MP2}}_{\mathrm{c}}(M)}{W^{\mathrm{PC}}_{\mathrm{c},\infty}(M)}\right)^{-1/2}\right) - \sum_{i}^{N} W^{\mathrm{PC}}_{\mathrm{c},\infty}(F_i)\left(1 - \left(1 + \frac{4\sum_i^N E^{\mathrm{MP2}}_{\mathrm{c}}(F_i)}{\sum_i^N W^{\mathrm{PC}}_{\mathrm{c},\infty}(F_i)}\right)^{-1/2}\right) \tag{16}$$

Before employing $\lambda^{\mathrm{SPL}}_{\mathrm{ext}}$ to test the accuracy of MP2 for weak interactions, we should note that $\lambda^{\mathrm{SPL}}_{\mathrm{ext}}$ is, in general, different from the exact λ_{ext} for the interaction energies since it uses the $\lambda = 1$ point from $W^{\mathrm{SPL,\,int}}_{\mathrm{c},\lambda}(M)$ (eq 15). In ref 48, it has been shown that the accuracy of the interaction energies arising from $W^{\mathrm{SPL,\,int}}_{\mathrm{c},\lambda}(M)$ is on average higher than that of MP2 for the S66 dataset. Particularly, in the case of dispersion complexes, the SPL accuracy is 2 times greater than that of MP2.[48] To meaningfully use $\lambda^{\mathrm{SPL}}_{\mathrm{ext}}$ as a predictor of the MP2 accuracy for weak interactions, we should also check whether the curvature of $W^{\mathrm{SPL,\,int}}_{\mathrm{c},\lambda}(M)$ is more accurate than its MP2 counterpart (the latter has zero curvature since MP2 approximates $W^{\mathrm{int}}_{\mathrm{c},\lambda}(M)$ by a straight line). By resorting to the available data, we can use the MP3 theory results for the S66 dataset to assess the accuracy of the $W^{\mathrm{SPL,\,int}}_{\mathrm{c},\lambda}(M)$ initial curvature. Even though the MP3 itself does not provide a striking improvement over MP2 for the S66 dataset,[53] by virtue of eq 7

$$E^{\mathrm{MP3,int}}_{\mathrm{c}} = \frac{1}{6}\frac{\partial^2 W^{\mathrm{int}}_{\mathrm{c},\lambda}}{\partial\lambda^2}\bigg|_{\lambda=0} \tag{17}$$

Hence, it provides the exact initial curvature of $W^{\mathrm{int}}_{\mathrm{c},\lambda}(M)$. In Figure 4, we compare the initial curvature of $W^{\mathrm{SPL,\,int}}_{\mathrm{c},\lambda}(M)$

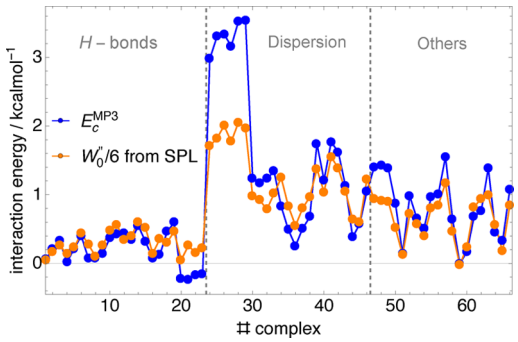

Figure 4. Plots comparing the initial curvature of the SPL AC interaction integrand (eq 13) with $E^{\mathrm{MP3}}_{\mathrm{c}}$ interaction energies of the S66 dataset (see eq 17).

(divided by 6) against the $E^{\mathrm{MP3}}_{\mathrm{c}}$ for the interaction energies of the S66 dataset taken from ref 53. To compute all input quantities needed for $W^{\mathrm{int}}_{\mathrm{c},\lambda}(M)$ pertaining to noncovalent datasets in this work, we employ the same basis set and other computational details as in ref 48. The underlying basis set is aug-cc-pVQZ enhanced with additional basis functions. For example, this basis set gives the MP2 interaction energies for the S66 dataset that are within the 1.5% agreement with their MP2/CBS extrapolated counterparts.

We can see from Figure 4 that the initial curvature of $W^{\mathrm{int}}_{\mathrm{c},\lambda}(M)$ is fairly approximated by the SPL, with an MAE of 0.31 kcal/mol (against $E^{\mathrm{MP3}}_{\mathrm{c}}$). From Figure 4, we can also see that the exact $W^{\mathrm{int}}_{\mathrm{c},\lambda}(M)$ is typically convex at $\lambda = 0$, except for 5

https://dx.doi.org/10.1021/acs.jctc.0c00049
J. Chem. Theory Comput. 2020, 16, 4141−4149

(20th−23th; 59th) out of 66 complexes. As discussed earlier, one would indeed expect $W^{\mathrm{int}}_{c,\lambda}(M)$ to be, most of the times, convex since MP2 with sufficiently large basis set typically overbinds complexes bonded by weak interactions. As it can be seen from Figure 4, four of these complexes belong to the "hydrogen bonds" subset of S66. In these four cases, the SPL mispredicts the sign of the initial curvature of the exact AC interaction integrand. However, on the positive side, the magnitude of E_c^{MP3} in these four cases is relatively small ($|E_c^{\mathrm{MP3}}| \leq 0.25$ kcal/mol) in comparison with complexes that have large positive curvature (24th−29th complex). In the case of 59th complex (belonging to "others"), the curvature is just slightly negative, and in this case, SPL gets the sign right. This shows that even though the SPL AC integrand for total energies (eq 11) is always convex, the SPL AC interaction integrand (eq 12) can also have a concave region.

As said, the MP2 interaction AC curve has always 0 curvature, and thus, its MAE/6 in predicting the curvature of $W^{\mathrm{int}}_{c,\lambda}(M)$ would be the averaged magnitude of E_c^{PT3}, which is 0.90 kcal/mol. Thereby, the MAE of SPL in predicting the initial curvature of $W^{\mathrm{int}}_{c,\lambda}(M)$ is 3 times smaller than that of MP2. For this reason, we expect that $\lambda_{\mathrm{ext}}^{\mathrm{SPL}}$ for the interaction energies arising from $W^{\mathrm{SPL},\,\mathrm{int}}_{c,\lambda}(M)$ to be in a fair agreement with its exact counterpart for weak interactions.

4.2. Results for the S22 and S66 Datasets. With eqs 15 and 16, we have what we need to compute $\lambda_{\mathrm{ext}}^{\mathrm{SPL}}$ corresponding to the HF AC for the interaction energies of molecular complexes bonded by noncovalent interactions. The principal point of $\lambda_{\mathrm{ext}}^{\mathrm{SPL}}$ is its use as an indicator for the accuracy of the MP2 theory. We define the MP2 accuracy predictor (MAP) in terms of $\lambda_{\mathrm{ext}}^{\mathrm{SPL}}$ of eq 15: MAP = $|1 - \lambda_{\mathrm{ext}}^{\mathrm{SPL}}|$ (distance from the physical $\lambda = 1$ point), making the MP2 error increase as the predictor increases. In Figure 5, we plot the relative error in the MP2 binding energies as a function of MAP for the S22 and S66 datasets. Note that only in one case from these two datasets $\lambda_{\mathrm{ext}}^{\mathrm{SPL}}$ was greater than 1 (just slightly though), and that is the 59th complex of the S66 dataset (see the previous subsection). The MAP values for each complex of the S22 and S66 datasets are reported in the Supporting Information.

From Figure 5, we can observe a general trend that the MP2 errors on an average decrease as MAP approaches 0 (i.e. the corresponding interaction AC curve becomes more linear). In both panels in Figure 5, we have added horizontal-dashed lines going through the relative errors of MP2 at 10 and 25%. This enables us to better understand how the MAP discriminates the MP2 errors, and we can distinguish the following three regions as follows:

(i) When MAP $\leq$ 0.19, the errors are typically small (in S66, they are always less than 7.5%, and here, we have 31 S66 complexes), and for these MAP values, MP2 calculations for weak interactions can be considered very reliable.

(ii) When MAP is between 0.19 and 0.21 (24 S66 complexes), the error can range from 2.5 to 25% in the S66. Thus, MP2 calculations for weak interactions with these MAP values should be treated with caution, yet based on the analysis here, the errors are expected to be less than 25%.

(iii) When MAP $\geq$ 0.21 (10 S66 complexes), the MP2 errors are large (always greater than 25% for the S66), and for stacking complexes for which MP2 failures are well known, they skyrocket (up to 80%). Thus, in these cases, MP2 calculations are not reliable and could be even qualitatively wrong.

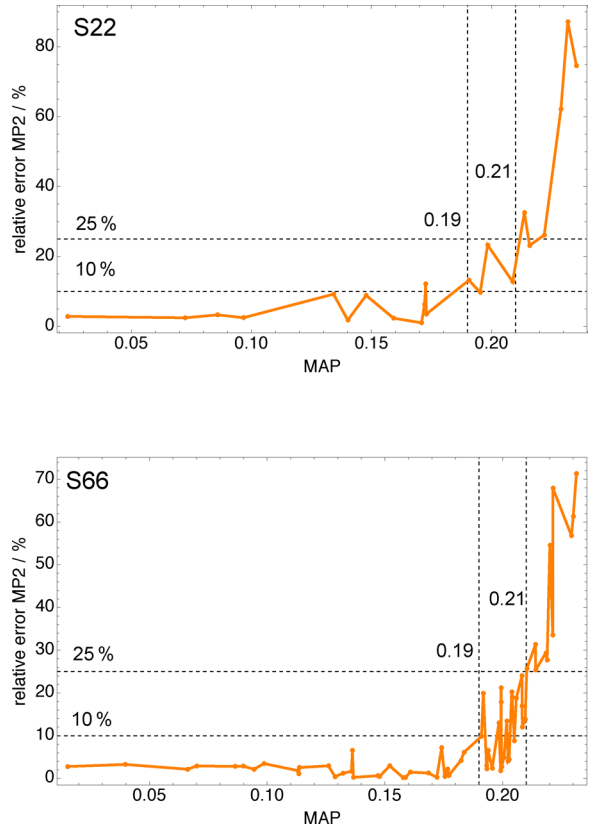

Figure 5. Relative errors in MP2 binding energies as a function of MAP for the S22 (top panel) and S66 (lower panel) datasets.

Also, to better visualize the second and third regions for the S66 dataset, in Figure 6, we show the same plot as in the bottom panel of Figure 5 but with an exponential scale on the x-axis.

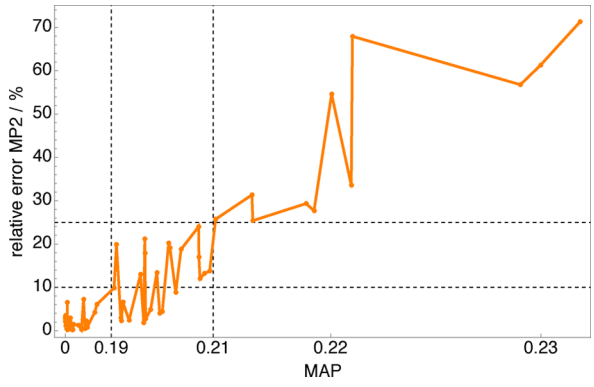

Figure 6. Same as the bottom panel of Figure 4 but with a different (exponential; $e^{58.4x}$) scale on the x-axis.

In Figure 7, we show the benzene dimer and acetic acid dimer AC curves obtained from eq 11 together with underlying MAP values; representing a situation when MP2 is accurate (the latter case) and when it is not (the former case). We also calculate MAE and MARE for the three subsets of the S66 dataset, and these are shown in Figure 8, as a function of averaged MAP pertaining to a given subset. For hydrogen

https://dx.doi.org/10.1021/acs.jctc.0c00049
J. Chem. Theory Comput. 2020, 16, 4141−4149

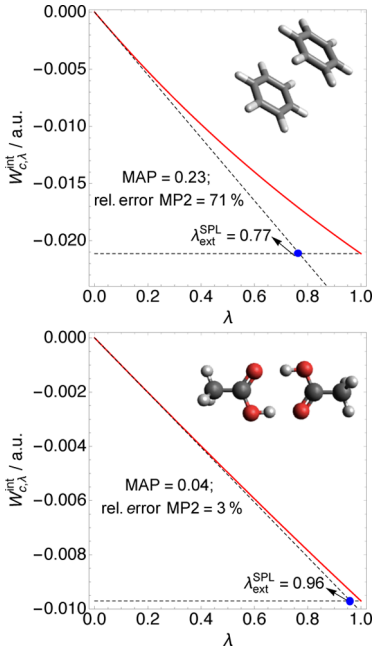

Figure 7. Interaction AC curves obtained by the SPL interpolation via eq 11 for the benzene dimer (upper panel) and the acetic acid dimer (lower panel).

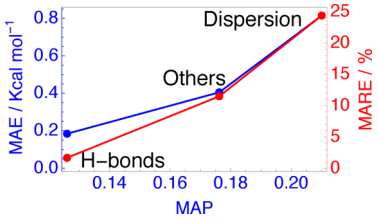

Figure 8. MARE and MAE for the MP2 method as a function of averaged MAP for the subsets of the S66 dataset.

bonded systems where the averaged MAP value is close to 0, the AC interaction curves are expected to be highly linear, and consequently, the MP2 is more accurate for these systems. We can observe in Figure 8 that MAP increases, as we go from H-bonded complexes, over complexes classified as "others" (those bonded by a combination of dispersion and electrostatics) to complexes bonded by dispersion. This indicates that the accuracy of MP2 decreases in this order.

In the original S66 publication, the authors have employed DFT-SAPT analysis to determine the ratio between the dispersion and electrostatic contribution to the interaction energy for each of the S66 complexes.[53] They found that the accuracy of MP2/CBS typically increases as the electrostatics/dispersion ratio increases. To relate their findings to our results that are shown in Figure 8, we plot MAP as a function of the dispersion/electrostatics ratio obtained by the DFT-SAPT energy decomposition. The plot is shown in Figure 9, and the values for the dispersion/electrostatics ratio for the S66 dataset have been taken from the original work.[53] We can see from Figure 9 that MAP increases and then saturates with the dispersion/electrostatics ratio. This indicates that the SPL interaction AC integrand becomes more linear as the dispersion component to the interaction energies decreases. By thinking reverse ("lower MP2 accuracy → more pronounced curvature of the exact interaction AC curve"),

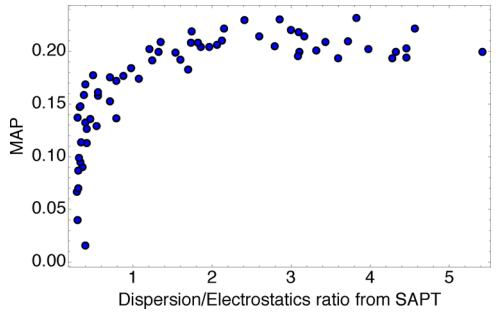

Figure 9. MAP as a function of the dispersion/electrostatics ratio of contributions to the interaction energies obtained from the DFT-SAPT energy decomposition for the complexes of the S66 dataset.

we can claim that the exact AC interaction curve also becomes more linear as the dispersion/electrostatics ratio decreases.

At least in a DFT context, Strømsheim et al. have shown that the exact AC integrand of the dispersion bonded He_2 is quite curved if one looks at the interaction energy, even though the AC integrand of the complex and monomers (He atom; which is also shown here) look quite linear.[54] Our analysis here shows that the dispersion interactions also make the curvature of the HF AC interaction integrand highly pronounced. In both HF and DFT theories, stronger curvature of the AC integrand is often interlinked with the presence of "non-dynamical" (static) electronic correlations.[23,24,44,45] However, our findings and that of Strømsheim et al. indicate that the dispersion interactions can have the same effect on the AC interaction integrands. This, in turn, mirrors the difficulties in perturbative treatments of both dispersion interactions and strong electronic correlations.

5. CONCLUSIONS AND OUTLOOK

In summary, we use the AC insights to better understand and predict the accuracy of PT2 theories. We also report the highly accurate HF AC curves for the helium isoelectronic series and compare them with their DFT counterparts. We transform the exact form of our λ_{ext} indicator into a practical tool (MAP) for predicting the accuracy of the MP2 method for systems that dissociate into fragments with nondegenerate ground states. A key point to note about the MAP predictor is that it practically comes at no additional computational cost. Computing it by means of eqs 15 and 16 requires only (beyond the MP2 calculation itself) $W_{\infty}^{PC}[\rho^{HF}]$, which is easily computed from $\rho^{HF}(\mathbf{r})$ and its gradient. This practical aspect of the MAP predictor, combined with its relevance for noncovalent interactions (NIs) and the popularity of MP2 methods for NIs, is even more useful in the light of recent findings of Furche and co-workers.[55] Namely, these authors have found that the performance of MP2 for NIs systematically worsens with the increase of a molecular size. Thus, they advise caution when MP2 is used for calculating NIs between large molecules, given that the results can be even qualitatively wrong. This is where our MAP can come into play, as it can gauge the reliability of such calculations (as shown in Figure 5.)

The MAP indicator is presently applicable to systems that dissociate into fragment with nondegenerate ground states. To address this, we will obtain exact AC curves for small covalently bonded diatomics, and then we will use these curves to get hints on how to transform the exact λ_{ext} into a practical indicator that also works for systems that dissociate into fragments with degenerate ground states.

https://dx.doi.org/10.1021/acs.jctc.0c00049
J. Chem. Theory Comput. 2020, 16, 4141−4149

In future work, we will also explore the possibility of defining and analyzing the local HF AC curves, as it has been done for their DFT counterparts.[23,24,44−56] This could prove useful in using the λ_{ext} indicator locally (i.e., at a given point in space).

APPENDIX

PC model and W_λ^{HF}

As explained in Section 4, while $W_{c,\lambda}^{SPL,\,int}(M)$ (l.h.s. of eq 13 is an accurate approximation to $W_{c,\lambda}^{int}(M)$ (r.h.s of eq 12) for NIs,[48] we do not expect the SPL scheme to accurately approximate the two terms on the r.h.s. of eq 12. Comparing the size of the MP2 and CCSD(T) total energies, we expect these two terms to have a concave adiabatic connection curve for λ between 0 and 1. On the other hand, we expect $W_{c,\lambda}^{int}(M)$ to be convex (given that MP2 overbinds a vast majority of S22 and S66 complexes). However, the difference between two SPL curves resulting from eq 12, which we use here to model $W_{c,\lambda}^{int}(M)$, can in principle also have concave regions. As such, it could also capture cases in which the interaction HF AC is concave. In practice, achieving this seems difficult. Namely, in the case of 20th−23th complexes of Figure 4, $W_{c,\lambda}^{int}(M)$ is convex, while its exact counterpart has negative initial curvature. A notable exception is the 59th complex of Figure 4 where $W_{c,\lambda}^{int}(M)$ correctly captures the negative initial curvature of the exact AC interaction integrand. As said, in all other S66 complexes, the initial curvature of $W_{c,\lambda}^{int}(M)$ is positive and that is captured by the SPL model of eq 12. Overall, the accuracy of the $W_{c,\lambda}^{SPL,\,int}(M)$ curve for NIs[48] results from an error cancellation between the complex and monomers. A similar error cancellation has been observed for the fixed-node error in Quantum Monte Carlo calculations of NIs.[57]

In this same light, we discuss in more details the use of $W_\infty^{PC}[\rho^{HF}]$ in the SPL interpolation scheme as an approximation to $W_\infty^{HF}[\rho^{HF}]$. The PC model was in the first place designed as an approximation to $W_\infty^{DFT}[\rho]$.[52,58] The key building block of this model is the PC cell, which provides a way to approximate the electrostatic potential of the exchange-correlation hole in the $\lambda \to \infty$ limit of DFT AC.[52,58] The PC cell is a sphere of uniform charge around an electron at $\mathbf{r}$, and its dipole moment, approximated in terms of the density gradient at $\mathbf{r}$, is set to zero. From the electrostatic potential of the PC cell, one obtains the gradient expansion approximation (GEA) expression for $W_\infty^{PC}[\rho]$ (eq 14). We note that the exact $W_\infty^{HF}[\rho^{HF}]$ is expected to be much lower than $W_\infty^{PC}[\rho^{HF}]$. This is because $W_\infty^{PC}[\rho]$ is energetically very close to the exact $W_\infty^{DFT}[\rho]$ (see refs 8 and 51), while the following inequality holds[36]

$$W_\infty^{HF}[\rho^{HF}] \le W_\infty^{DFT}[\rho^{HF}] + 2E_x^{HF}[\rho^{HF}] \tag{18}$$

Thus, one can even think of approximating W_∞^{HF} with $W_\infty^{\beta=2}$ where

$$W_\infty^{\beta}[\rho^{HF}] = W_\infty^{PC}[\rho^{HF}] + \beta E_x^{HF}[\rho^{HF}] \tag{19}$$

Despite this reasoning, the accuracy of SPL interaction energies changes very little when we approximate W_∞^{HF} with $W_\infty^{\beta}[\rho^{HF}]$ and vary β from 0 to 2. We illustrate this in Figure A1, which shows the MAE for the S66 dataset of the SPL interpolation as a function of β when we set $W_\infty^{HF}[\rho^{HF}] = W_\infty^{\beta}[\rho^{HF}]$. We can see from Figure A1 that the MAE changes just slightly as β goes from 0 to 2, and the MAE at $\beta = 2$ is even slightly higher than at $\beta = 0$. For this reason, we use the "bare" PC model (i.e., $W_\infty^{\beta=0}[\rho^{HF}]$ as an approximation to $W_\infty^{HF}[\rho^{HF}]$ throughout this work).

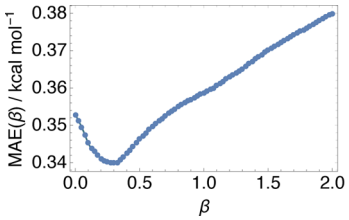

Figure A1. MAE for the S66 dataset of the SPL interpolation scheme as a function of β where we set $W_\infty^{HF}[\rho^{HF}] = W_\infty^{\beta}[\rho^{HF}]$ (eq 19).

ASSOCIATED CONTENT

Supporting Information

The Supporting Information is available free of charge at https://pubs.acs.org/doi/10.1021/acs.jctc.0c00049.

Construction of the Ψ_λ^{HF} wavefuntion for two-electron systems (Section 3), fitting functions for DFT AC curves plotted in Figure 2, and discussion, in more details, the use of eq 13, MAP values for each complex of the S22 and S66 datasets (Figure4) (PDF)

AUTHOR INFORMATION

Corresponding Author

Stefan Vuckovic − *Department of Chemistry, University of California, Irvine, California 92697, United States;* orcid.org/0000-0002-0768-9176; Email: svuckovi@uci.edu

Authors

Eduardo Fabiano − *Institute for Microelectronics and Microsystems (CNR-IMM), Via Monteroni, Campus Unisalento, Lecce 73100, Italy;* orcid.org/0000-0002-3990-669X

Paola Gori-Giorgi − *Department of Theoretical Chemistry and Amsterdam Center for Multiscale Modeling, FEW, Vrije Universiteit, Amsterdam 1081HV, The Netherlands;* orcid.org/0000-0002-5952-1172

Kieron Burke − *Department of Chemistry, University of California, Irvine, California 92697, United States*

Complete contact information is available at: https://pubs.acs.org/10.1021/acs.jctc.0c00049

Notes

The authors declare no competing financial interest.

ACKNOWLEDGMENTS

S.V. acknowledges funding from the Rubicon project (019.181EN.026), which is financed by the Netherlands Organisation for Scientific Research (NWO). K.B. acknowledges funding from NSF (CHE 1856165). P.G.G. acknowledges funding from the European Research Council under H2020/ERC Consolidator Grant corr-DFT (grant no. 648932) and from NWO under Vici grant 724.017.001.

REFERENCES

(1) Pauli, W. Principles of wave mechanics. *Handbuch der Physik;* Springer: 1933, *24*, 162.

(2) Hellman, H. *Einführung in die Quantenchemie*; Franz Deuticke: Leipzig, 1937, 285.

https://dx.doi.org/10.1021/acs.jctc.0c00049
J. Chem. Theory Comput. 2020, 16, 4141−4149

(3) Feynman, R. P. Forces in Molecules. *Phys. Rev.* **1939**, *56*, 340−343.
(4) Harris, J.; Jones, R. O. The surface energy of a bounded electron gas. *J. Phys. F: Met. Phys.* **1974**, *4*, 1170.
(5) Langreth, D. C.; Perdew, J. P. The exchange-correlation energy of a metallic surface. *Solid State Commun.* **1975**, *17*, 1425−1429.
(6) Gunnarsson, O.; Lundqvist, B. I. Exchange and correlation in atoms, molecules, and solids by the spin-density-functional formalism. *Phys. Rev. B* **1976**, *13*, 4274.
(7) Savin, A.; Colonna, F.; Pollet, R. Adiabatic Connection Approach to Density Functional Theory of Electronic Systems. *Int. J. Quantum Chem.* **2003**, *93*, 166.
(8) Vuckovic, S.; Wagner, L. O.; Mirtschink, A.; Gori-Giorgi, P. Hydrogen Molecule Dissociation Curve with Functionals Based on the Strictly Correlated Regime. *J. Chem. Theory Comput.* **2015**, *11*, 3153−3162.
(9) Liu, Z.-F.; Burke, K. Adiabatic connection in the low-density limit. *Phys. Rev. A* **2009**, *79*, No. 064503.
(10) Vuckovic, S.; Levy, M.; Gori-Giorgi, P. Augmented potential, energy densities, and virial relations in the weak- and strong-interaction limits of DFT. *J. Chem. Phys.* **2017**, *147*, 214107.
(11) Pernal, K. Correlation energy from random phase approximations: A reduced density matrices perspective. *Int. J. Quantum Chem.* **2018**, *118*, No. e25462.
(12) Pernal, K. Electron Correlation from the Adiabatic Connection for Multireference Wave Functions. *Phys. Rev. Lett.* **2018**, *120*, No. 013001.
(13) Becke, A. D. Density-functional thermochemistry. III. The role of exact exchange. *J. Chem. Phys.* **1993**, *98*, 5648.
(14) Perdew, J. P.; Ernzerhof, M.; Burke, K. Rationale for mixing exact exchange with density functional approximations. *J. Chem. Phys.* **1996**, *105*, 9982−9985.
(15) Zhao, Y.; Schultz, N. E.; Truhlar, D. G. Design of density functionals by combining the method of constraint satisfaction with parametrization for thermochemistry, thermochemical kinetics, and noncovalent interactions. *J. Chem. Theory Comput.* **2006**, *2*, 364−382.
(16) Grimme, S. Semiempirical hybrid density functional with perturbative second-order correlation. *J. Chem. Phys.* **2006**, *124*, No. 034108.
(17) Goerigk, L.; Grimme, S. Efficient and Accurate Double-Hybrid-Meta-GGA Density Functionals- Evaluation with the Extended GMTKN30 Database for General Main Group Thermochemistry, Kinetics, and Noncovalent Interactions. *J. Chem. Theory Comput.* **2010**, *7*, 291−309.
(18) Sharkas, K.; Toulouse, J.; Savin, A. Double-hybrid density-functional theory made rigorous. *J. Chem. Phys.* **2011**, *134*, No. 064113.
(19) Ernzerhof, M. Construction of the adiabatic connection. *Chem. Phys. Lett.* **1996**, *263*, 499.
(20) Seidl, M.; Perdew, J. P.; Kurth, S. Simulation of all-order density-functional perturbation theory, using the second order and the strong-correlation limit. *Phys. Rev. Lett.* **2000**, *84*, 5070.
(21) Mori-Sánchez, P.; Cohen, A. J.; Yang, W. Many-electron selfinteraction error in approximate density functionals. *J. Chem. Phys.* **2006**, *125*, 201102.
(22) Becke, A. D. Density functionals for static, dynamical, and strong correlation. *J. Chem. Phys.* **2013**, *138*, No. 074109.
(23) Vuckovic, S.; Irons, T. J. P.; Savin, A.; Teale, A. M.; Gori-Giorgi, P. Exchange− correlation functionals via local interpolation along the adiabatic connection. *J. Chem. Theory Comput.* **2016**, *12*, 2598−2610.
(24) Vuckovic, S.; Irons, T. J. P.; Wagner, L. O.; Teale, A. M.; Gori-Giorgi, P. Interpolated energy densities, correlation indicators and lower bounds from approximations to the strong coupling limit of DFT. *Phys. Chem. Chem. Phys.* **2017**, *19*, 6169−6183.
(25) Bahmann, H.; Zhou, Y.; Ernzerhof, M. The shell model for the exchange-correlation hole in the strong-correlation limit. *J. Chem. Phys.* **2016**, *145*, 124104.
(26) Vuckovic, S.; Gori-Giorgi, P. Simple fully nonlocal density functionals for electronic repulsion energy. *J. Phys. Chem. Lett.* **2017**, *8*, 2799−2805.
(27) Gould, T.; Vuckovic, S. Range-separation and the multiple radii functional approximation inspired by the strongly interacting limit of density functional theory. *J. Chem. Phys.* **2019**, *151*, 184101.
(28) Vuckovic, S. Density functionals from the multiple-radii approach: analysis and recovery of the kinetic correlation energy. *J. Chem. Theory Comput.* **2019**, *15*, 3580−3590.
(29) Burke, K.; Ernzerhof, M.; Perdew, J. P. The adiabatic connection method: A nonempirical hybrid. *Chem. Phys. Lett.* **1997**, *265*, 115.
(30) Møller, C.; Plesset, M. S. Note on an Approximation Treatment for Many-Electron Systems. *Phys. Rev.* **1934**, *46*, 618−622.
(31) Pastorczak, E.; Pernal, K. Correlation Energy from the Adiabatic Connection Formalism for Complete Active Space Wave Functions. *J. Chem. Theory Comput.* **2018**, *14*, 3493−3503.
(32) Pernal, K. Exact and approximate adiabatic connection formulae for the correlation energy in multireference ground and excited states. *J. Chem. Phys.* **2018**, *149*, 204101.
(33) Lee, T. J.; Taylor, P. R. A diagnostic for determining the quality of single-reference electron correlation methods. *Int. J. Quantum Chem.* **1989**, *36*, 199−207.
(34) Janssen, C. L.; Nielsen, I. M. B. New diagnostics for coupled-cluster and Møller− Plesset perturbation theory. *Chem. Phys. Lett.* **1998**, *290*, 423−430.
(35) Deng, J.; Gilbert, A. T. B.; Gill, P. M. W. Diagnostics of molecular orbital quality. *Can. J. Chem.* **2010**, *88*, 754−758.
(36) Seidl, M.; Giarrusso, S.; Vuckovic, S.; Fabiano, E.; Gori-Giorgi, P. Communication: Strong-interaction limit of an adiabatic connection in Hartree-Fock theory. *J. Chem. Phys.* **2018**, *149*, 241101.
(37) Görling, A.; Levy, M. Correlation-energy functional and its high-density limit obtained from a coupling-constant perturbation expansion. *Phys. Rev. B* **1993**, *47*, 13105.
(38) Görling, A.; Levy, M. Exact Kohn-Sham scheme based on perturbation theory. *Phys. Rev. A* **1994**, *50*, 196.
(39) Cremer, D. Møller−Plesset perturbation theory: from small molecule methods to methods for thousands of atoms. *Wiley Interdiscip. Rev.: Comput. Mol. Sci.* **2011**, *1*, 509−530.
(40) Grimme, S. Improved second-order Møller−Plesset perturbation theory by separate scaling of parallel-and antiparallel-spin pair correlation energies. *J. Chem. Phys.* **2003**, *118*, 9095−9102.
(41) Jung, Y.; Lochan, R. C.; Dutoi, A. D.; Head-Gordon, M. Scaled opposite-spin second order Møller−Plesset correlation energy: an economical electronic structure method. *J. Chem. Phys.* **2004**, *121*, 9793−9802.
(42) Neese, F.; Schwabe, T.; Kossmann, S.; Schirmer, B.; Grimme, S. Assessment of orbital-optimized, spin-component scaled second-order many-body perturbation theory for thermochemistry and kinetics. *J. Chem. Theory Comput.* **2009**, *5*, 3060−3073.
(43) Dunning, T. H., Jr. Gaussian basis sets for use in correlated molecular calculations. I. The atoms boron through neon and hydrogen. *J. Chem. Phys.* **1989**, *90*, 1007.
(44) Teale, A. M.; Coriani, S.; Helgaker, T. The calculation of adiabatic-connection curves from full configuration-interaction densities: Two-electron systems. *J. Chem. Phys.* **2009**, *130*, 104111.
(45) Teale, A. M.; Coriani, S.; Helgaker, T. Accurate calculation and modeling of the adiabatic connection in density functional theory. *J. Chem. Phys.* **2010**, *132*, 164115.
(46) Seidl, M.; Perdew, J. P.; Levy, M. Strictly correlated electrons in density-functional theory. *Phys. Rev. A* **1999**, *59*, 51.
(47) Fabiano, E.; Gori-Giorgi, P.; Seidl, M.; Della Sala, F. Interaction-Strength Interpolation Method for Main-Group Chemistry: Benchmarking, Limitations, and Perspectives. *J. Chem. Theory Comput.* **2016**, *12*, 4885−4896.
(48) Vuckovic, S.; Gori-Giorgi, P.; Della Sala, F.; Fabiano, E. Restoring size consistency of approximate functionals constructed from the adiabatic connection. *J. Phys. Chem. Lett.* **2018**, 3137.

https://dx.doi.org/10.1021/acs.jctc.0c00049
J. Chem. Theory Comput. 2020, 16, 4141−4149

(49) Giarrusso, S.; Gori-Giorgi, P.; Della Sala, F.; Fabiano, E. Assessment of interaction-strength interpolation formulas for gold and silver clusters. *J. Chem. Phys.* **2018**, *148*, 134106.
(50) Seidl, M.; Gori-Giorgi, P.; Savin, A. Strictly correlated electrons in density-functional theory: A general formulation with applications to spherical densities. *Phys. Rev. A* **2007**, *75*, No. 042511.
(51) Kooi, D. P.; Gori-Giorgi, P. Local and global interpolations along the adiabatic connection of DFT: a study at different correlation regimes. *Theor. Chem. Acc.* **2018**, *137*, 166.
(52) Seidl, M.; Perdew, J. P.; Kurth, S. Density functionals for the strong-interaction limit. *Phys. Rev. A* **2000**, *62*, No. 012502.
(53) Řezáč, J.; Riley, K. E.; Hobza, P. S66: A well-balanced database of benchmark interaction energies relevant to biomolecular structures. *J. Chem. Theory Comput.* **2011**, *7*, 2427−2438.
(54) Strømsheim, M. D.; Kumar, N.; Coriani, S.; Sagvolden, E.; Teale, A. M.; Helgaker, T. Dispersion interactions in density-functional theory: An adiabatic-connection analysis. *J. Chem. Phys.* **2011**, *135*, 194109.
(55) Nguyen, B. D.; Chen, G. P.; Agee, M. M.; Burow, A. M.; Tang, M. P.; Furche, F. Divergence of Many-Body Perturbation Theory for Noncovalent Interactions of Large Molecules. *J. Chem. Theory Comput.* **2020**, 2258.
(56) Irons, T. J. P.; Teale, A. M. The coupling constant averaged exchange−correlation energy density. *Mol. Phys.* **2015**, *114*, 484−497.
(57) Dubecký, M.; Mitas, L.; Jurečka, P. Noncovalent Interactions by Quantum Monte Carlo. *Chem. Rev.* **2016**, *116*, 5188−5215.
(58) Mirtschink, A.; Seidl, M.; Gori-Giorgi, P. Energy Densities in the Strong-Interaction Limit of Density Functional Theory. *J. Chem. Theory Comput.* **2012**, *8*, 3097.

https://dx.doi.org/10.1021/acs.jctc.0c00049
J. Chem. Theory Comput. 2020, 16, 4141−4149